OUTSTANDING SYMPOSIUM PAPERS

Articles in this section are based on presentations that were selected by MRS Meeting Symposium Organizers as outstanding papers. Upon selection, authors are invited to submit their research results to Journal of Materials Research. *These papers are subject to the same peer review and editorial standards as all other JMR papers. This is another way by which the Materials Research Society recognizes high quality papers presented at its meetings.*

Analysis of indentation creep

Don S. Stone[a)]
Department of Materials Science and Engineering, and Materials Science Program, University of Wisconsin–Madison, Madison, Wisconsin 53706

Joseph E. Jakes
Materials Science Program, University of Wisconsin–Madison, Madison, Wisconsin 53706; and Performance Enhanced Biopolymers, United States Forest Service, Forest Products Laboratory, Madison, Wisconsin 53726

Jonathan Puthoff
Materials Science Program, University of Wisconsin–Madison, Madison, Wisconsin 53706

Abdelmageed A. Elmustafa
Department of Mechanical Engineering and The Applied Research Center–Jefferson Laboratory, Old Dominion University, Norfolk, Virginia 23529

(Received 25 November 2009; accepted 22 January 2010)

Finite element analysis is used to simulate cone indentation creep in materials across a wide range of hardness, strain rate sensitivity, and work-hardening exponent. Modeling reveals that the commonly held assumption of the hardness strain rate sensitivity (m_H) equaling the flow stress strain rate sensitivity (m_σ) is violated except in low hardness/modulus materials. Another commonly held assumption is that for self-similar indenters the indent area increases in proportion to the (depth)^2 during creep. This assumption is also violated. Both violations are readily explained by noting that the proportionality "constants" relating (i) hardness to flow stress and (ii) area to (depth)^2 are, in reality, functions of hardness/modulus ratio, which changes during creep. Experiments on silicon, fused silica, bulk metallic glass, and poly methyl methacrylate verify the breakdown of the area-(depth)^2 relation, consistent with the theory. A method is provided for estimating area from depth during creep.

I. INTRODUCTION

Materials scientists have long relied on indentation creep to study rate-sensitive deformation in solids.[1–3] Although not as straight-forward to analyze and interpret as the more conventional uniaxial creep experiment, the indentation test is nevertheless easier to perform, especially when the specimen is too small to grip for uniaxial testing. Over the years the great majority of work in indentation creep has been performed at high homologous temperatures where the yield stress is a small fraction of the Young's modulus. These kinds of experiments have motivated theoretical treatments to address the relationship between indentation and uniaxial creep under conditions where the elastic deformations are small and therefore relatively unimportant.[2,4–6]

This research is motivated by the desire to investigate low-temperature, rate-sensitive deformation in high hardness/modulus (H / E^*) materials like refractory coatings and bulk metallic glasses (BMGs). Although one does not normally think of hard materials as creeping at low temperatures, such materials do exhibit time- and temperature-dependent flow behavior near the yield stress, and this behavior carries within it information about the deformation mechanisms.[7] The time-dependent behavior is readily manifested in an indentation hardness test, which thereby offers an experimenter the unique capability to study deformation kinetics in hard, brittle materials because it can produce deformation without fracture.

This investigation differs from the earlier theoretical studies on low H / E^* materials because in the materials now under consideration, the elastic components of the deformation can be quite large. For low H / E^* materials, the indentation creep properties are not sensitive to modulus, so the modulus can be neglected in a theoretical

[a)]Address all correspondence to this author.
e-mail: dsstone@wisc.edu

This paper was selected as an Outstanding Symposium Paper for the 2007 MRS Fall Meeting, Symposium AA Proceedings, Vol. 1049.
DOI: 10.1557/JMR.2010.0092

analysis. For high H / E^* materials modulus effects must be taken into account for a proper analysis.

In experimental studies of indentation creep it is often assumed that the strain rate sensitivity of the hardness (m_H) equals that of the flow stress (m_σ) and that the square root of the projected area of the indent, $\sqrt{A}$, increases in proportion to indentation depth, h_i, defined in Sec. II, during creep (e.g., Refs. 8 and 9). These key assumptions lead to a convenient, closed-form solution for the depth as a function of time, thereby allowing the experimenter to back out the material parameter m_σ from a depth-versus-time trace. However, there is no theoretical justification for such assumptions. In this work, we therefore test them using a combination of finite element analysis and nanoindentation experiments on high H / E^* materials.

II. PRELIMINARIES

There are different ways of controlling the indenter to measure rate-sensitive deformation. In indentation creep the indenter is first driven into the specimen to a predetermined load or depth, and the load is then held constant for a period of time prior to unloading. During the hold the indenter continues to penetrate, and as it does the area of the indent increases, so the hardness drops. As the hardness drops, the rate of penetration decreases, and in this way the experiment sweeps out a spectrum of hardness versus indentation strain rate, the slope of which on a log–log scale gives m_H. Other methods for measuring m_H include indentation load relaxation,[10] in which the depth is held fixed and the load is allowed to relax; indentation rate-change, in which the specimen is first loaded at one rate and then partially unloaded, then reloaded at a second rate[11]; and constant indentation strain rate that measures the hardness at fixed $\dot{L}/L$, where L is the load.[12] In the Appendix, we construct an analysis to handle creep and load relaxation. Because the constant load creep test is the easiest and most commonly used experiment, the remainder of the work focuses exclusively on this experiment. Under some conditions at least, indentation creep, indentation load relaxation, and indentation rate-change give the same results.[11]

A schematic load-depth trace from an indentation creep experiment is shown in Fig. 1. During the loading and constant load creep portions of the experiment, the instantaneous hardness, H, is defined as the instantaneous load divided by the instantaneous projected contact area,

$$H(t) = \frac{P(t)}{A(t)} \quad . \tag{1}$$

An indentation strain rate, $\dot{\varepsilon}_H$, can be specified based on any dimension of the indent that increases with time; we use

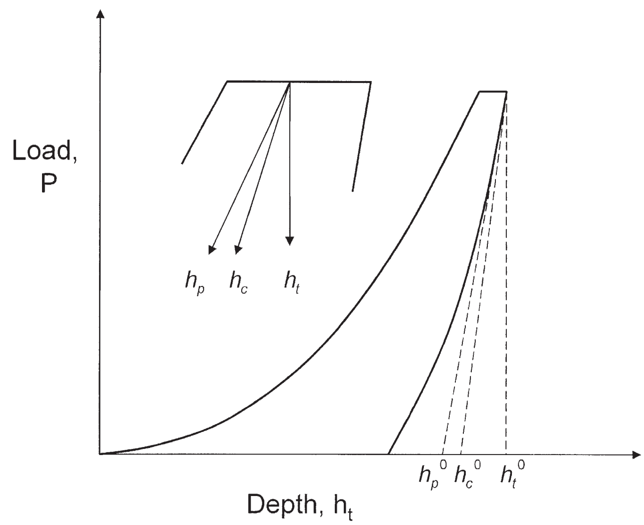

FIG. 1. Load–depth curve illustrating constant load creep along with the different definitions of indentation depth: h_t^0, h_c^0, and h_p^0 are the total, contact, and plastic depths, respectively, at the end of creep. These parameters can be measured directly from a load-depth trace. At any time during or before creep, the instantaneous values are h_t, h_c, and h_p. These, along with the instantaneous contact area, may be estimated based on the analysis presented in this work.

$$\dot{\varepsilon}_H = \frac{d \ln \sqrt{A}}{dt} \quad . \tag{2}$$

The strain rate sensitivity of the hardness is

$$m_H = \left. \frac{\partial \ln H}{\partial \ln \dot{\varepsilon}_H} \right|_{h_p} \quad , \tag{3}$$

where the derivative is taken at fixed depth to eliminate the effects of an indentation size effect, if any.[11,13] In indentation creep the results of the analysis for strain rate sensitivity do not depend appreciably on which characteristic length of the indent (e.g., total depth, square root of area) is used to define strain rate.[14] However, for indentation load relaxation in which $\dot{h}_t = 0$ even though plastic deformation is taking place, it makes more sense to use $\sqrt{A}$ for the basis for calculating strain rate.

For comparison, the strain rate sensitivity of the flow stress is defined as

$$m_\sigma = \left. \frac{\partial \ln \sigma}{\partial \ln \dot{\varepsilon}} \right|_{\varepsilon} \quad , \tag{4}$$

where m_σ can be measured in tension, compression, or shear using a rate-change or load relaxation experiment. Fixing the strain during the experiment helps to ensure that the strain rate sensitivity is isostructural, which means that increases in flow stress caused by work hardening are excluded in the measurement.

From Eqs. (1) and (2) it should be evident that for an accurate analysis of creep data the growth of the area of the indent during creep must be identified. One way to do this is to use the dynamic stiffness method in which a small alternating current (ac) signal is superimposed on the applied load to allow the stiffness of contact, which is proportional to $\sqrt{A}$, to be determined continuously throughout the experiment.[15] We shall use this method for some of the experiments on fused silica described below. Another way to determine $A(t)$ during creep is to estimate it from the load-depth-time trace. Stone and Yoder[11] proposed a method for performing this estimate. With their method the total depth of indentation (h_t) is separated into plastic (h_p) and elastic (h_e) components following the Doerner and Nix[16] approach of extrapolating the top portion of the unloading curve directly back to zero load (Fig. 1). The area of the indent is assumed to be a function of plastic depth: $A = A(h_p)$. Although for the vast majority of nanoindentation studies the Doerner–Nix definition of plastic depth has been superceded by the Oliver–Pharr[17] contact depth, h_c, there is no fundamental reason why h_p cannot be used as the basis for calculating areas, and our experiments suggest that h_p might often be better for analyzing creep than h_c. Even the total depth, h_t, can be used as a basis for estimating $A(t)$. The main differences between using the different depth measures to estimate area arise from the different ways elastic displacements are subtracted out in the analysis. In our analysis these differences are rigorously handled through the power law exponents ζ_i ($i = t, p, c$) introduced below.

The different depth measures are illustrated in Fig. 1. The values of these parameters, h_t^0, h_c^0, and h_p^0, at the end of the constant load portion, can all be obtained directly from the unloading portion of the load–depth curve. The corresponding instantaneous h_t, h_c, and h_p (inset) are defined based on the assumption that the unloading slope could be measured if the test were interrupted. In the absence of stiffness measurements to determine the instantaneous area during indentation creep, the trick to analyzing indentation creep is then to estimate this area based on instantaneous h_t, h_c, or h_p in Fig. 1. In turn, h_c and h_p cannot be measured directly, but must themselves be estimated using methods derived in the Appendix. At constant hardness the area scales in proportion to the square of each of h_t, h_c, and h_p. But during a creep test the hardness changes with depth, so the proportionality breaks down. In the new terminology, the exponents relating $\sqrt{A}$ to the different h_i at constant load are called ζ_i, and these generally differ from 1.

In the Appendix, we revise the earlier analysis.[11] Guided by the results of finite element modeling described in Sec. III, (i) we no longer require for $\sqrt{A}$ to increase directly proportional to depth for cone- and pyramid-shaped indenters, but instead by a power law; and (ii) we expand the original analysis based on h_p so that h_c and h_t, too, can be used to determine $A(t)$.

III. FINITE ELEMENT ANALYSIS SIMULATIONS

The finite element simulations have been reported in detail elsewhere.[14] These simulations used the elasto-plastic features of ABAQUS finite element code (Simulia, Warwick, RI) to model the penetration of a conical indenter into a substrate. The indenter and solid were modeled as bodies of revolution to take advantage of axisymmetry. The indenter was a perfectly rigid cone with an inclined face angle of 22.5°. The sample was modeled as a semi-infinite, elastic–plastic von Mises material, using quadrilateral axisymmetric four-node isoparametric elements. Meshes were generated using GENMESH2D, and multipoint constraints (MPCs) were created using GENMPC2D. The mesh was further refined in regions near the edge of contact to minimize the discrete displacement effects during relaxation.

The contact between indenter and sample was modeled as having a friction coefficient, μ, varying from 0.0 to 0.5.[18] To simulate a variety of material behaviors we adopted a strain-hardening creep law given by

$$\dot{\varepsilon}^{cr} = \left(\kappa\sigma^n\left[(m+1)\varepsilon^{cr}\right]^m\right)^{\frac{1}{m+1}} \quad , \tag{5}$$

where n, m are the stress and the strain exponents. κ is a rate parameter. By adjusting κ while keeping n and m constant, it is possible to tailor the hardness of the material while maintaining a fixed strain rate sensitivity [$m_\sigma = (m + 1)/n$] and work-hardening exponent ($\chi = -m\ /\ n$). This constitutive relation can obviously model steady-state power law creep ($m = 0$); it can also model other behaviors over modest ranges of strain rate in situations where the strain rates can be approximated as power law functions of stress. The reason for including strain hardening in the constitutive model is to identify whether it influences m_H.[14]

The indentation process was simulated in four sequential steps. In the first step, contact between indenter tip and sample was established. Next, the indenter was pushed into the sample under a load that increased parabolically throughout 1 s. In the third step, the load on the tip was held constant for 2 to 3 s (this is the indentation creep portion of the experiment). The last step consisted of pulling the indenter out of the sample over a period of about 1 s.

The hardness versus strain rate curves generated for materials with the same strain rate sensitivity m_σ (same m, n) but with different hardness (different κ) are shown in Fig. 2. The slopes of the curves, which correspond to m_H, are all different, leading us to conclude that in general $m_H \neq m_\sigma$. Nevertheless, the slopes approach m_σ as the hardness decreases, and we find that the ratio of $m_H\ /\ m_\sigma$ is a unique function of $H\ /\ E^*$ and is independent of the other material properties as shown in Fig. 3. The data in Figs. 2 and 3 are taken from simulations with frictionless indenter-specimen contact; the addition of friction,

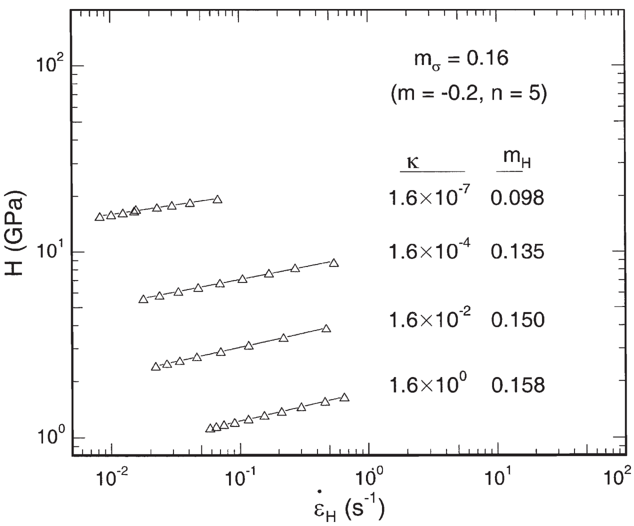

FIG. 2. Hardness-strain rate data generated from computer simulations employing finite element analysis. The units of κ are GPa^{-5} s$^{-0.8}$.

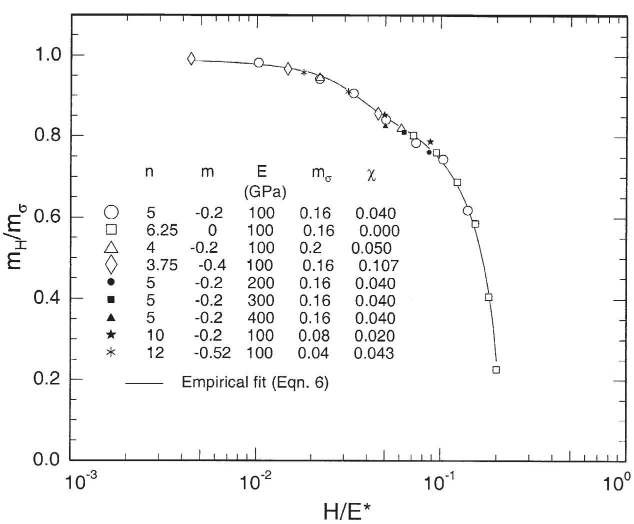

FIG. 3. Effect of hardness level on strain rate sensitivity of the hardness.

however, does not appreciably affect the results.[18] The continuous curve in Fig. 3 is an empirical fit of the data given by

$$m_H/m_\sigma \cong \left[0.91 - 0.057\arctan\left(\frac{\log(x/28.2)}{0.2}\right)\right] \times \sqrt{1-(x/0.21)^2} \quad , \qquad (6)$$

where $x = H / E^*$. Using Eq. (6), it is possible to correct a measurement of m_H to obtain m_σ.

With finite element analysis it is possible to calculate $H(t)$ using the load and area as direct outputs of the simulations. In a real experiment only the load and depth can be measured directly, and the area must be determined indirectly. Dynamic stiffness measurements can be used to determine the area[19]; but experimenters usu-

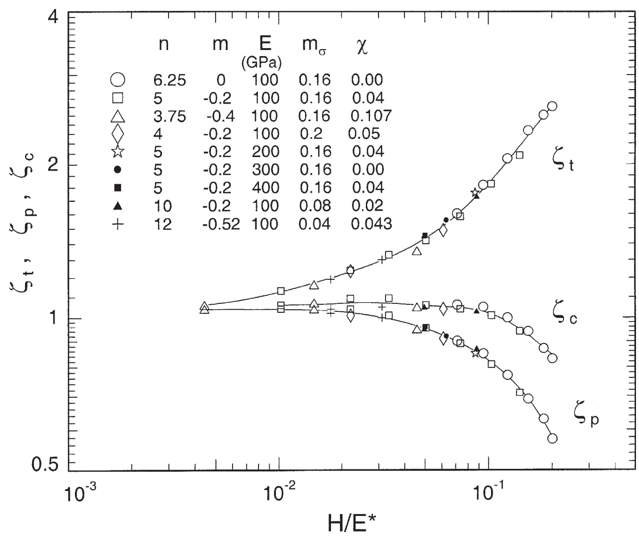

FIG. 4. Exponents relating $\sqrt{A}$ to depth (h_t, h_p, h_c) during indentation creep. The solid lines are empirical (spline) fits. Based on the theory presented in the paper, these curves can be algebraically manipulated and integrated to construct the theory curves in Fig. 5.

ally estimate the change in area during creep based on an increase in depth, assuming that the area is proportional to the square of depth.[8,9] This latter practice is open to dispute. For instance, Rar and coworkers[20] have reported that the area-(depth)^2 law is violated during creep, an assertion that is supported by our work. We define the parameter $\zeta_i = \partial \ln \sqrt{A} / \partial \ln h_i|_P$, where h_i is the measure of depth being used to estimate area. In practice, it is possible to use total measured depth, h_t, plastic depth, h_p,[16] or contact depth, h_c to estimate the area during creep.[17] A plot of the ζ_i determined from simulations of different materials at zero friction is shown in Fig. 4. Interestingly, all of the data fall along master curves, but only for low H / E^* do all of the ζ_i approach 1. For $H / E^* < 0.04$ ζ_p is closest to 1 (approximately 1.03). For hardness higher than $0.04E^*$, ζ_c is closest to 1.

IV. DISCUSSION OF FINITE ELEMENT ANALYSIS SIMULATION RESULTS

Finite element analysis reveals that the strain rate sensitivity of the hardness, m_H, differs from that of the flow stress, m_σ, except at low H / E^* (Fig. 3). It also reveals that for constant load creep with a cone-shaped indenter, $\sqrt{A}$ increases in proportion to the depth h_p, h_c, or h_t, raised to a power other than 1, in contrast to what one might anticipate given the self-similar geometry of the indenter (Fig. 4). The significance of these two results is that the measurement of rate-sensitive deformation in hard materials is more complicated than a simplistic analysis might suggest. Fortunately, both results are systematic and easy to understand, so that it remains possible to work around them in the analysis and interpretation of indentation creep data.

The trend in m_H / m_σ, Fig. 3, is independent of work hardening and strain rate sensitivity[14] as well as friction.[18] Instead, the trend is primarily caused by the proportionality factor between hardness and flow stress, i.e., k in $H = k\sigma^{\mathrm{eff}}$, which is not a constant but depends instead upon the ratio σ^{eff} / E^* (see, e.g., Ref. 21). Our previous analysis[14] shows that in a creep test, as the flow stress beneath the specimen evolves due to changes in deformation rate, so does the ratio k. Kermouche and coworkers[22,23] have independently arrived at a similar conclusion. The changes in hardness that take place during indentation creep are therefore related not only to changes in σ^{eff} but also to changes in k. Working with logarithms, we may designate these changes as

$$\Delta \ln H = \Delta \ln \sigma^{\mathrm{eff}} + \Delta \ln k = \left(1 + \frac{d \ln k}{d \ln (\sigma^{\mathrm{eff}}/E^*)}\right) \Delta \ln \sigma^{\mathrm{eff}} \quad . \tag{7}$$

For low σ^{eff} / E^* materials, k is independent of σ^{eff} / E^*, in which case $\Delta \ln H = \Delta \ln \sigma^{\mathrm{eff}}$. In this instance $m_H = m_\sigma$. For elastic materials with H / E^* approaching 0.21 in simulations for the cone geometry, the hardness becomes proportional to E^* rather than σ^{eff}, so that the second term in parentheses in Eq. (7) approaches -1, in which case $\Delta \ln H$ (and therefore m_H) goes to zero.

In a hardness measurement with a pyramid- or cone-shaped indenter, the average strain rate beneath the indenter is proportional to $\dot{\varepsilon}_H$ as defined above, and the average strain is proportional to the tangent of the angle between indenter and specimen surface.[24,25] Earlier results suggest that these other proportionality factors, like k, also depend on H / E^*, and that to account for the detailed shape of the m_H / m_σ curve in Fig. 3 it is necessary to take them into account.[14] Nevertheless, the overall tendency of m_H / m_σ to approach zero at high H / E^* in Fig. 3 is simply because the higher hardness materials are becoming increasingly elastic so that the right side of Eq. (7) approaches zero.

Likewise, the trends in the different ζ_i, Fig. 4, can also be explained by noting how the elasticity of the solid affects the ratios of $\sqrt{A}/h_i$. For instance, we may suppose

$$\sqrt{A} = C^i h_i \quad (i = t, p, \text{ or } c) \quad , \tag{8}$$

where the C^i depend on H / E^*. Because H changes during a creep experiment, so do the C^i. Working with logarithms, we identify the change in $\sqrt{A}$ as arising from both a change in depth and a change in H / E^*:

$$\Delta \ln \sqrt{A} = \frac{d \ln C^i}{d \ln (H/E^*)} \Delta \ln H + \Delta \ln h_i \quad . \tag{9}$$

At constant load $\Delta \ln H = -2 \Delta \ln \sqrt{A}$; algebraic manipulation of Eq. (9) leads to

$$\frac{d \ln C^i}{d \ln (H/E^*)} = \frac{1}{2}\left(\frac{1}{\zeta_i} - 1\right) \quad . \tag{10}$$

To verify this relationship, we show data of C^p, C^t, and C^c in Fig. 5. These data were generated by taking the ratios of $\sqrt{A^0}$ at the end of creep to the depths at the end of creep (i.e., h_t^0, h_c^0, h_p^0) from all of the different simulations. The lines in Fig. 5 for C^i-versus-H / E^* ("theory") have been generated by taking spline fits of the ζ_i-versus-H / E^* data (lines in Fig. 4), then incorporating them into Eq. (10) and integrating. Our ability to accomplish this feat proves that values of ζ_i in Fig. 4 come from the trends in C^i with hardness. Interestingly, there is a significant amount of scatter in the C^i for small H / E^* in Fig. 5. This scatter is due to the influence of pileup, which is sensitive to the work hardening and strain rate sensitivity properties of the materials in addition to the ratio H / E^*.[26] In comparison there is relatively little scatter in ζ_i for low H / E^*, which suggests that while pileup might affect the ratio C^i, pileup has little effect on the derivative $d \ln \sqrt{A}/d \ln h_p$ for cone-shaped indenters. This result suggests that the C^i can be written as a product of functions, one depending solely on H / E^*, and the other depending on other parameters such as friction and the work hardening and strain rate sensitivity exponents. We conclude that for indentation creep at constant load, the deviations of the ζ_i away from 1 are caused by the changes taking place in C^p, C^t, and C^c as hardness is lowered during creep.

The Appendix provides mathematical formulas for estimating instantaneous area during creep. For instance, with formulas (A5) and (A3) ($i = p$) it is possible to calculate the area from a load-depth trace provided that

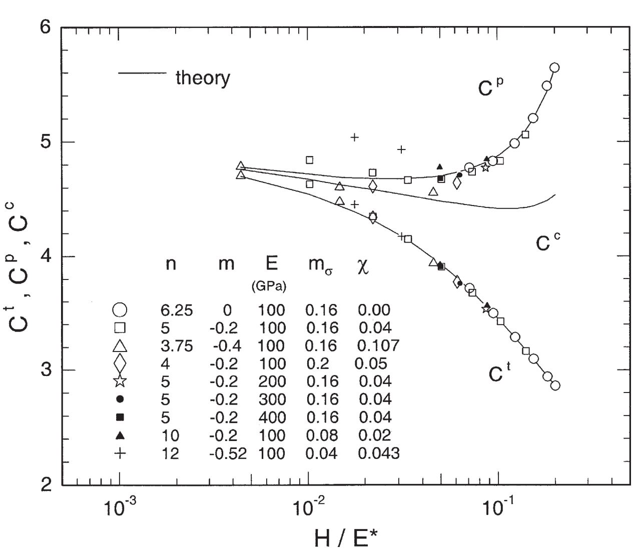

FIG. 5. Proportionality factors relating $\sqrt{A}$ to depth (h_t, h_p, h_c) at constant hardness, from simulated hardness tests on different materials. The theory lines are calculated from the lines in Fig. 4 with the help of Eq. (10).

ζ_p is known. Likewise, Eq. (A3) ($i = t$) can be used if ζ_t is known, and Eqs. (A7) and (A3) ($i = c$) can be used if ζ_c is known. The different ζ_i can, in turn, be garnered either from theory (e.g., Fig. 4) or by fitting the area–depth curves generated from these formulas to experimental data. The formulas based on different ζ_i are equivalent; the choice of which to use is up to the discretion of the practitioner. Using ζ_t and Eq. (A3) is the simplest approach from a computational standpoint.

The Appendix formulas have been derived using first order Taylor series approximations, so it helps to test them by comparing them with the output of finite element analysis simulations. For the purpose of illustration we use the method that uses ζ_p. In this case for formulas (A5) and (A3) to be useful they should be able to replicate the area-depth profile when ζ_p is used as a fitting parameter. Furthermore, the best fit ζ_p-value should agree with the ζ_p-value generated directly from finite element analysis output (Fig. 4). Comparisons are shown in Fig. 6 for two materials. Curve A is from a relatively elastic material ($H / E^* \approx 0.15$; $n = 0.5$, $m = -0.2$), while curve B is for a relatively plastic material ($H / E^* \approx 0.015$; $n = 3.75$, $m = -0.4$). From the load-depth traces (inset) the relevant parameters for A are $P^0 = P = 6.51 \times 10^{-5}$ N, $1 / A^0\ E_{\mathrm{eff}} = 8472$ N/m, $h_{\mathrm{p}}^0 = 12.8$ nm, and $h_{\mathrm{t}}^0 = 20.5$ nm. For B they are $P^0 = P = 8.03 \times 10^{-6}$ N, $1 / A^0\ E_{\mathrm{eff}} = 9379$ N/m, $h_{\mathrm{p}}^0 = 15.2$ nm, and $h_{\mathrm{t}}^0 = 16.1$ nm. The best fit values of ζ_p are 0.73 and 1.03 for materials A and B, respectively. If substituted into Eqs. (A5) and (A3) the best fit parameters give

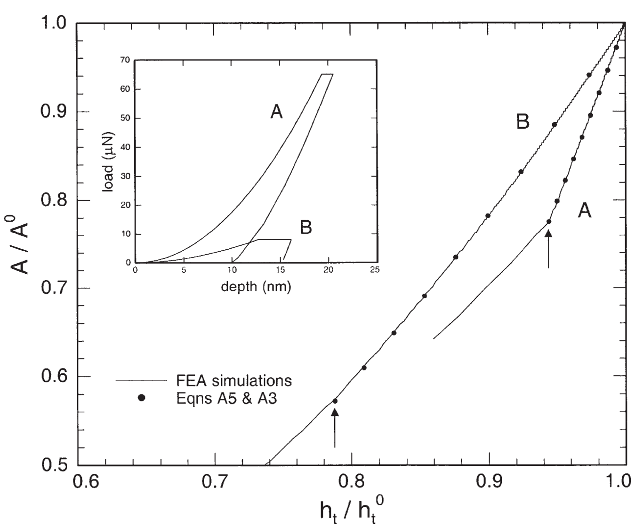

FIG. 6. Instantaneous area versus depth curves generated from finite element analysis. (A^0 and h_t^0 are, respectively, the area and depth at end of creep.) The solid lines are obtained directly from the output based on radius of contact. The data points (most of which have been omitted for clarity sake) are obtained indirectly based on the approximations in Eqs. (A5) and (A3). The arrows point to the beginning of the constant load portion of the area-depth trace.

$$\frac{h_{\mathrm{p}}}{h_{\mathrm{p}}^{\ 0}} = 2.838\left(\frac{h_{\mathrm{t}}}{h_{\mathrm{t}}^{\ 0}}\right) - 1.838 \quad , \qquad \text{(A5A)}$$

and

$$\frac{A}{A^0} = \left(\frac{h_{\mathrm{p}}}{h_{\mathrm{p}}^{\ 0}}\right)^{1.46} \quad , \qquad \text{(A3A)}$$

for material A; and

$$\frac{h_{\mathrm{p}}}{h_{\mathrm{p}}^{\ 0}} = 1.121\left(\frac{h_{\mathrm{t}}}{h_{\mathrm{t}}^{\ 0}}\right) - 0.121 \quad , \qquad \text{(A5B)}$$

and

$$\frac{A}{A^0} = \left(\frac{h_{\mathrm{p}}}{h_{\mathrm{p}}^{\ 0}}\right)^{2.06} \quad , \qquad \text{(A3B)}$$

for material B. The formulas, represented by the dots in Fig. 6, work remarkably well in their ability to replicate the area–depth curves. Furthermore, the best fit values of ζ_p are close to the values of 0.71 (Material A) and 1.04 (Material B) generated directly as output from the finite element analysis simulations, Fig. 4. We conclude that formulas (A3) and (A5) are accurate enough to handle large changes in area without having to rely on unreasonable values of ζ_p to do so.

V. EXPERIMENTS INVESTIGATING THE AREA-DEPTH RELATION DURING CREEP

Indentation creep experiments were performed to evaluate the ζ_i for comparison with finite element analysis predictions, Fig. 4. Materials studied included a BMG $Zr_{45}Cu_{48}Al_7$, poly methyl methacrylate (PMMA), fused silica, and (100)-silicon. All of these have high H / E^* ratios. With the exception of silicon, all lack an indentation size effect, and even in silicon the size effect is weak. Yielding in amorphous solids is known to be pressure sensitive (e.g., Refs. 27 and 28), so the BMG, PMMA, and fused silica all violate the von Mises assumption of our finite element model. It is not known how this difference might affect the behavior.

The BMG specimen was made by casting a 3-mm-diameter ingot in a vacuum apparatus from pure components. The glassy nature of the specimen was verified by differential scanning calorimetry, XRD, and dark-field transmission electron microscopy. Its surface was ground and polished to 0.01-μm alumina[29] prior to testing. The PMMA specimen was a nanoindentation standard obtained from Hysitron Inc. (Minneapolis, MN) and was tested in the as-received condition. Fused-silica calibration standards were obtained from MTS (Oak Ridge, TN) and Hysitron, and the silicon wafer was obtained from Polishing Corporation of America (Santa Clara, CA).

Most of the testing was performed on a Hysitron Triboindenter. Using this instrument, we subjected the BMG, PMMA, fused silica, and silicon specimens to a novel kind of experiment that we call broadband nanoindentation creep (BNC).[29] With BNC it is possible to obtain hardness-strain rate data spanning 4–5 decades of strain rate from a single indent. The indenter is loaded into the specimen as quickly as possible (0.01–0.05 s), held at constant load for intervals ranging between 0.01 and 50 s, and then unloaded (beyond about 50–200 s hold time it becomes difficult to correct for instrumental drift). The data collection rate of the Triboindenter is high enough to capture strain rates extending up to 10/s–100/s; however, for correct data analysis it is necessary to account for low-pass filters acting on the displacement signal.[30] The component of filtering arising from the spring-mass-damping system is relatively minor because the indenter is in contact with the specimen. The details of the BNC experiment are described elsewhere.[29]

Indentation creep measurements were also performed on a fused-silica calibration standard using an MTS Nanoindenter XP. The experiments consisted of first loading the indenter into the specimen, holding the load constant for 20 s, and then unloading. The instantaneous projected contact area was determined based on dynamic contact stiffness measured continuously during the creep portion of the experiment.

For experiments performed with the Triboindenter, residual indents were imaged and the areas measured with a Quesant (Agoura Hills, CA) atomic force microscope (AFM) incorporated in the Triboindenter. The AFM was operated in contact mode and calibrated using an Advanced Surface Microscopy, Inc. (Indianapolis, IN) calibration standard with a pitch of 292 ± 0.5 nm. The AFM was calibrated separately for 4- and 10-μm field of view images. Individual 4-μm field of view images were made for the BMG, fused silica, and silicon specimens and 10 μm for the PMMA. Image analysis software ImageJ was used to manually measure the projected contact areas from the AFM images as described in a previous publication.[31,32] The ImageJ software website is found at (http://rsb.info.nih.gov/ij/).

One might reasonably question whether the areas of residual indents measured following removal of load might differ from the areas under load. Sakai and Nakano[33] found that for Vickers indents in soda-lime glass and PMMA the areas remain unchanged. To test whether the same holds true for Berkovitch indents in PMMA, which has a viscoelastic response, we repeatedly measured the profile of an indent at different times between 2 min and 5 days following a test and found that although the indent gradually becomes shallower, its lateral dimensions remain the same. We therefore assume in our analysis below that the indent areas remain unchanged for all materials other than fused silica. For fused silica, which is the most elastic of all the materials studied here, it has been shown that the areas of indents increase on unloading,[34] which might explain a discrepancy in our fused silica data, detailed below.

Area versus time data from the BMG are shown in Fig. 7 for a series of BNC tests run for different lengths of time. Individual data points were obtained by measuring the areas of the different indents. The lines were calculated from depth-load-time data based on Eqs. (A3) and (A5) in the Appendix. The hardness/modulus ratio for these glasses is about 0.075–0.085, corresponding to a predicted value of $\zeta_p \approx 0.88$ from Fig. 4. We find that $\zeta_p = 0.95$ works best, as represented by the labeled curve in Fig. 7. Additional curves representing $\zeta_p = 1.10$ and 0.80 are also shown to illustrate the limits of uncertainty.

Another way to identify the exponents ζ_i is to measure them directly from area versus depth at constant load. Figures 8(a) and 8(b) show $\sqrt{A^0}$-h_i^0 data from interrupted experiments on fused silica and PMMA, respectively. Duplicate experiments were performed at three different loads. The results were found to be independent of load, consistent with lack of an indentation size effect in these materials. The dashed lines in Fig. 8 have slopes of 1 on a log scale, which verify the proportionalities between $\sqrt{A}$ and the various h_i at fixed hardness. The data at constant load depict slopes (ζ_i) that differ from 1. Because PMMA tends to creep more, it exhibits larger differences in area depending on creep time and therefore less relative scatter in the data. The construction of the "theory" line shown next to the deepest indents in PMMA is based on Eq. (10) as described below.

Area-depth data from fused silica obtained using an MTS nanoindenter with continuous stiffness measurement

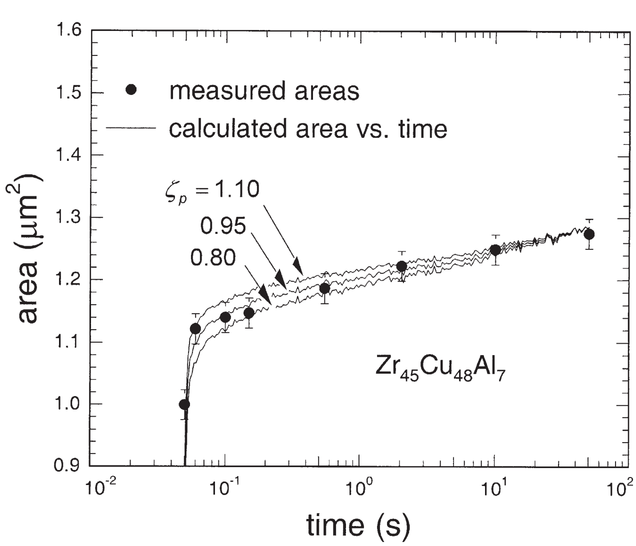

FIG. 7. Area versus time data from indentation creep of BMG. The measured areas (data points) were obtained directly using AFM and inferred from unloading stiffness. The lines are obtained using Eqs. (A5) and (A3).

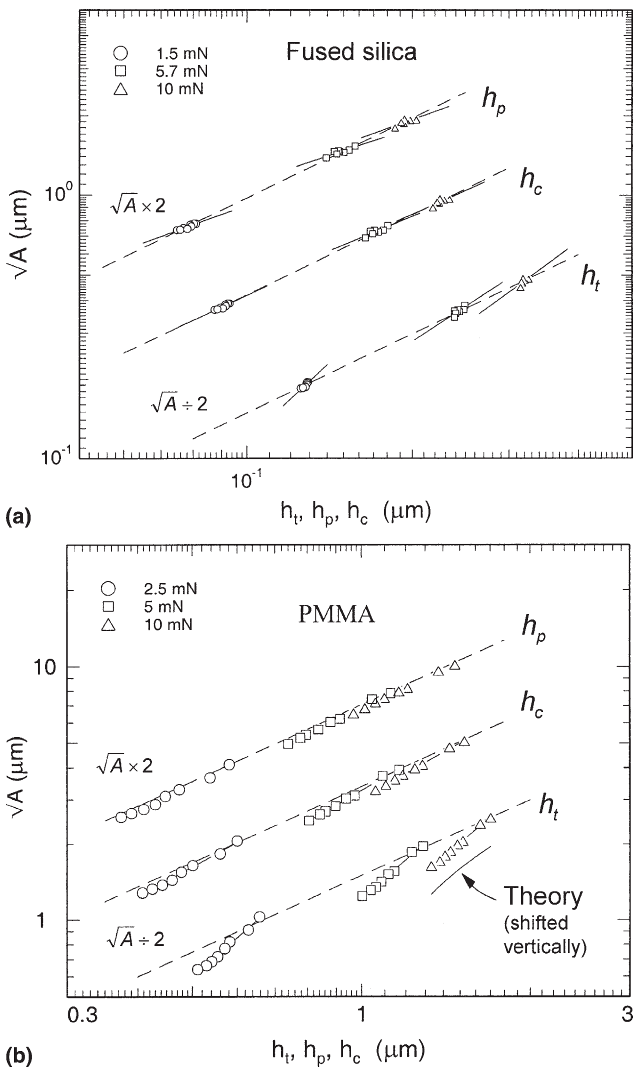

FIG. 8. Area-depth data for fused silica and PMMA. The dashed lines have slope 1 corresponding to the power law relation between $\sqrt{A}$ and h_i at constant hardness. The individual curves have slopes ζ_i, which generally differ from 1. For PMMA the theoretical prediction based on the results of finite element modeling is also shown.

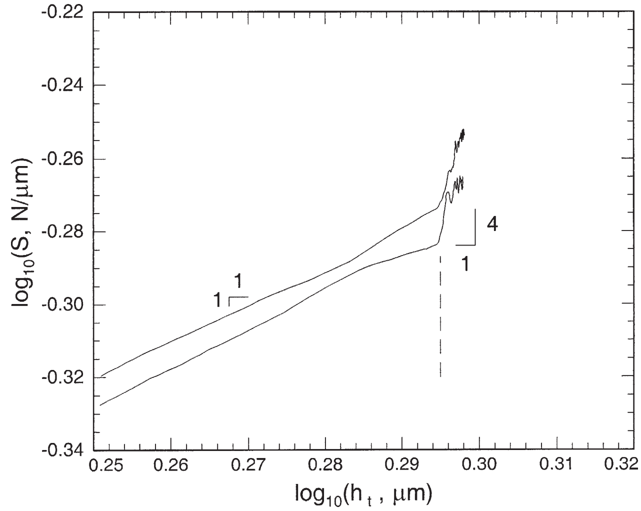

FIG. 9. Stiffness-depth data from indentation creep of silica obtained using CSM. Stiffness is proportional to $\sqrt{A}$.

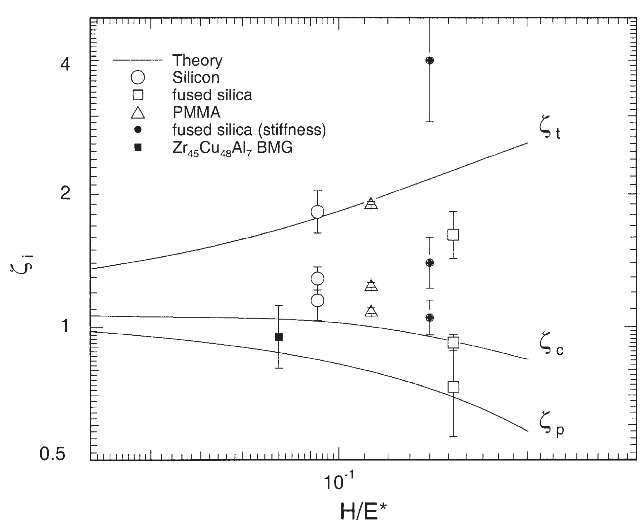

FIG. 10. Comparison between theory and experiment for power law exponent relating $\sqrt{A}$ to depth (h_t, h_c, h_p). For each material (excepting the BMG) the three data points correspond to ζ_t, ζ_c, and ζ_p in descending order (i.e., ζ_p is the lowest data point). For the BMG, only ζ_p was determined. The error bars represent standard error due to random sampling.

capabilities are shown in Fig. 9. The experimental details are described in Ref. 18. Here, the area of the indent is determined using contact stiffness. It is seen that during loading, the square root of area (stiffness) increases in proportion to the displacement; but once creep starts the power law relating depth to area increases to about $\zeta_t = 4 \pm 1.5$. This value for ζ_t is substantially higher than what we observe by measuring the areas directly, $\zeta_t = 1.6 \pm 0.2$, Fig. 8(a). The difference between the two methods might lie in the interpretation of continuous stiffness measurement data or in the measurement of indent areas in fused silica, for which it has been shown that the areas increase during unloading.[34]

The values of the ζ_i measured for fused silica, PMMA, and the $Zr_{45}Cu_{47}Al_8$ BMG are all compared with the results from the finite element models in Fig. 10. The lines in this figure are redrawn from Fig. 4. The data agree qualitatively with the model, but the uncertainties are too large to assess the precision to which the model predicts the behaviors of individual materials. The most reliable data are from PMMA, for which changes in area are large and therefore easy to measure. It is interesting to note that the experimental data generally fall at higher values for ζ_p and ζ_c than the theoretical results. This discrepancy might be a result of the fact that in the experiments a three-sided pyramid was used, while in the simulations the indenter was a cone.

Because of their relatively high quality resulting from the large change in area, the data for PMMA deserve more scrutiny. With these data H goes from about 0.16 E^* at the beginning of creep to about 0.05 E^* at the end (E^* = 6.34 GPa). Inspection of the ζ_t curve in Fig. 4 over this range of hardness suggests that ζ_t should decrease as the area grows larger, a behavior that should give rise to a downward curvature in the $\sqrt{A}$-versus-h_{t} data in Fig. 8. We can make the prediction of the theory more quantitative by using it to generate theoretical curves in Fig. 4 over the relevant range of hardness. The (H / E^*, ζ_t) curve in Fig. 4 is first converted to (A, ζ_t) based on knowledge of E^* and the load. From this it is a simple matter to numerically evaluate the integral

$$\ln h_{\mathrm{t}} = \int \frac{1}{\zeta_t} d \ln \sqrt{A} + const \quad , \qquad (11)$$

where the integration constant establishes the value of C^t. The slope and shape of the resulting theory line are consistent with the experimental PMMA data. It is not clear from the experimental data whether they have a downward or upward curvature, but even in the theoretical curve the downward curvature is relatively small, so we should not expect to easily detect the curvature in an experiment.

VI. SUMMARY

An analysis of indentation creep at constant load has been performed. The strain rate sensitivity of the hardness generally differs from that of the flow stress. The growth of the area of the indent with respect to depth differs from what it does during loading. Fortunately, with both situations the trends are insensitive to work hardening, creep, and friction, and the trends in behavior can be understood in terms of how the elastic–plastic problem depends on the ratio H / E^*. Experiments to measure the growth of the area with depth show results that are consistent with the finite element analysis simulations. Formulas for estimating the area from load and depth data during a creep or load relaxation experiment have been provided. This knowledge helps in the measurement and interpretation of rate-sensitive deformation using nanoindentation.

ACKNOWLEDGMENTS

A.A. Elmustafa wishes to thank the Summer Faculty Fellowship Research Program Office of Research, Old Dominion University Grant No. 993003. Research (D.S. Stone) sponsored by the National Science Foundation (Award CMMI-0824719).

NOMENCLATURE

Symbol	Definition
A	Instantaneous projected contact area
A^0	Projected contact area at the end of creep, immediately prior to unloading
β	Numerical factor relating E_{eff} to E^* (See E_{eff})
C^i	Ratio of $\sqrt{A}$ to depth of the ith type ($i = t, p, c$); [Eq. (8)]
χ	Work-hardening exponent in the finite element constitutive model ($= -m / n$)
Δ	Referring to a change in a quantity (e.g., $\Delta \ln A$)
E	Specimen Young's modulus
E^*	Hertzian contact modulus = $E / (1 - \nu^2)$ for rigid indenter
E_{eff}	Effective contact modulus = βE^*; $\beta \approx 1.23$
$\in$	Shape parameter in Oliver–Pharr contact depth
ε	Strain in a uniaxial experiment
$\dot{\varepsilon}$	Uniaxial strain rate in a conventional experiment
$\varepsilon^{\mathrm{cr}}$	Plastic strain in the finite element model
$\dot{\varepsilon}^{\mathrm{cr}}$	Plastic strain rate in the finite element constitutive model
$\dot{\varepsilon}_H$	Indentation strain rate [Eq. (2)]
H	Instantaneous Meyer hardness
h_{t}	Instantaneous total depth
h_{t}^0	Total depth at the end of creep, immediately prior to unloading
h_{p}	Instantaneous Doerner–Nix plastic depth [Eq. (A1)]
h_{p}^0	Plastic depth at the end of creep, immediately prior to unloading
h_{c}	Instantaneous Oliver–Pharr contact depth [Eq. (A6)]
h_{c}^0	Contact depth at the end of creep, immediately prior to unloading
k	$H / \sigma_{\mathrm{eff}}$
κ	Rate parameter in the finite element constitutive model
m_σ	Strain rate sensitivity of the flow stress [Eq. (4)]
m_H	Strain rate sensitivity of the hardness [Eq. (3)]
m, n	Power law exponents in the finite element constitutive model
ν	Poisson's ratio of specimen
P	Instantaneous (time-dependent) load
P^0	Load at the end of creep, immediately prior to unloading
S	Contact stiffness ($= E_{\mathrm{eff}} \sqrt{A}$)
σ	Stress in a uniaxial experiment
σ_{eff}	Representative flow stress in the plastic zone
x	H / E^*
ζ_i	Power law exponents relating A to h_i ($i = t, p, c$) for creep at constant load

REFERENCES

1. A.G. Atkins, A. Silverio, and D. Tabor: Indentation hardness and creep of solids. *J. Inst. Met.* **94**(Part 11), 369 (1966).
2. S.N.G. Chu and J.C.M. Li: Impression creep: A new creep test. *J. Mater. Sci.* **12**(11), 2200 (1977).

3. T.O. Mulhearn and D. Tabor: Creep and hardness of metals: A physical study. *J. Inst. Met.* **89,** 7 (1960).
4. Y-T. Cheng and C-M. Cheng: Scaling, dimensional analysis, and indentation measurements. *Mater. Sci. Eng., R* **44**(4–5), 91 (2004).
5. A.F. Bower, N.A. Fleck, A. Needleman, and N. Ogbonna: Indentation of a power law creeping solid. *Proc. R. Soc. London, Ser. A* **1993**(441), 97 (1911).
6. R. Hill: Similarity analysis of creep indentation tests. *Proc. R. Soc. London, Ser. A* **1992**(436), 617 (1898).
7. U.F. Kocks, A.S. Argon, and M.F. Ashby: Thermodynamics and kinetics of slip, in *Progress in Materials Science*, Vol. 19 (Pergamon Press, New York, 1975).
8. D. Jang and M. Atzmon: Grain-size dependence of plastic deformation in nanocrystalline Fe. *J. Appl. Phys.* **93**(11), 9282 (2003).
9. F. Wang, P. Huang, and K.W. Xu: Time dependent plasticity at real nanoscale deformation. *Appl. Phys. Lett.* **90**(16), 161921 (2007).
10. S.P. Hannula, D. Stone, and C.Y. Li: Determination of time-dependent plastic properties of metals by indentation load relaxation techniques, in *Electronic Packaging Materials Science*, edited by E.A. Giess, K-N. Tu, and D.R. Uhlmann (Mater. Res. Soc. Symp. Proc. **40,** Pittsburgh, PA, 1985), pp. 217–224.
11. D.S. Stone and K.B. Yoder: Division of the hardness of molybdenum into rate-dependent and rate-independent components. *J. Mater. Res.* **9**(10), 2524 (1994).
12. B.N. Lucas and W.C. Oliver: Time dependent indentation testing at non-ambient temperatures utilizing the high temperature mechanical properties microprobe, in *Thin Films: Stresses and Mechanical Properties V*, edited by S.P. Baker, C.A. Ross, P.H. Townsend, C.A. Volkert, and P. Børgesen (Mater. Res. Soc. Symp. Proc. **356,** Pittsburgh, PA, 1995), p. 645.
13. M.F. Tambwe, D.S. Stone, A.J. Griffin, H. Kung, Y.C. Lu, and M. Nastasi: Haasen plot analysis of the Hall-Petch effect in Cu–Nb nanolayer composites. *J. Mater. Res.* **14**(2), 407 (1999).
14. A.A. Elmustafa, S. Kose, and D.S. Stone: The strain-rate sensitivity of the hardness in indentation creep. *J. Mater. Res.* **22**(4), 926 (2007).
15. W.C. Oliver and G.M. Pharr: Measurement of hardness and elastic modulus by instrumented indentation: Advances in understanding and refinements to methodology. *J. Mater. Res.* **19**(1), 3 (2004).
16. M.F. Doerner and W.D. Nix: A method for interpreting the data from depth-sensing indentation instruments. *J. Mater. Res.* **1**(4), 601 (1986).
17. W.C. Oliver and G.M. Pharr: Improved technique for determining hardness and elastic modulus using load and displacement sensing indentation experiments. *J. Mater. Res.* **7**(6), 1564 (1992).
18. A.A. Elmustafa and D.S. Stone: Strain rate sensitivity in nanoindentation creep of hard materials. *J. Mater. Res.* **22**(10), 2912 (2007).
19. D.L. Goldsby, A. Rar, G.M. Pharr, and T.E. Tullis: Nanoindentation creep of quartz, with implications for rate- and state-variable friction laws relevant to earthquake mechanics. *J. Mater. Res.* **19**(1), 357 (2004).
20. A. Rar, S. Sohn, W.C. Oliver, D.L. Goldsby, T.E. Tullis, and G.M. Pharr: On the measurement of creep by nanoindentation with continuous stiffness techniques, in *Fundamentals of Nanoindentation and Nanotribology III*, edited by K.J. Wahl, N. Huber, A.B. Mann, D.F. Bahr, and Y-T. Cheng (Mater. Res. Soc. Symp. Proc. **841,** Warrendale, PA, 2005), R4.2.
21. K.L. Johnson: *Contact Mechanics* (Cambridge University Press, Cambridge, UK, 1985), p. 452.
22. G. Kermouche, J.L. Loubet, and J.M. Bergheau: Cone indentation of time-dependent materials: The effects of the indentation strain rate. *Mech. Mater.* **39**(1), 24 (2007).
23. G. Kermouche, J.L. Loubet, and J.M. Bergheau: A new index to estimate the strain rate sensitivity of glassy polymers using conical/pyramidal indentation. *Philos. Mag.* **86**(33–35), 5667 (2006).
24. M. Sakai, T. Akatsu, S. Numata, and K. Matsuda: Linear strain hardening in elastoplastic indentation contact. *J. Mater. Res.* **18**(9), 2087 (2003).
25. D. Tabor: *The Hardness of Metals* (Clarendon Press, Oxford, UK, 1951).
26. A. Bolshakov and G.M. Pharr: Influences of pileup on the measurement of mechanical properties by load and depth-sensing indentation techniques. *J. Mater. Res.* **13**(4), 1049 (1998).
27. R. Quinson, J. Perez, M. Rink, and A. Pavan: Yield criteria for amorphous glassy polymers. *J. Mater. Sci.* **32**(5), 1371 (1997).
28. C.A. Schuh and T.G. Nieh: A survey of instrumented indentation studies on metallic glasses. *J. Mater. Res.* **19**(1), 46 (2004).
29. J.B. Puthoff, J.E. Jakes, H. Cao, and D.S. Stone: Investigation of thermally activated deformation in amorphous PMMA and Zr–Cu–Al bulk metallic glasses with broadband nanoindentation creep. *J. Mater. Res.* **24**(3), 1279 (2009).
30. S.A.S. Asif, K.J. Wahl, R.J. Colton, and O.L. Warren: Quantitative imaging of nanoscale mechanical properties using hybrid nanoindentation and force modulation. *J. Appl. Phys.* **90**(3), 1192 (2001).
31. J.E. Jakes, C.R. Frihart, J.F. Beecher, R.J. Moon, P.J. Resto, Z.H. Melgarejo, O.M. Suarez, H. Baumgart, A.A. Elmustafa, and D.S. Stone: Nanoindentation near the edge. *J. Mater. Res.* **24**(3), 1016 (2009).
32. J.E. Jakes, C.R. Frihart, J.F. Beecher, R.J. Moon, and D.S. Stone: Experimental method to account for structural compliance in nanoindentation measurements. *J. Mater. Res.* **23**(4), 1113 (2008).
33. M. Sakai and Y. Nakano: Elastoplastic load–depth hysteresis in pyramidal indentation. *J. Mater. Res.* **17**(8), 2161 (2002).
34. J.H. Strader, S. Shim, H. Bei, W.C. Oliver, and G.M. Pharr: An experimental evaluation of the constant relating the contact stiffness to the contact area in nanoindentation. *Philos. Mag.* **86** (33–35), 5285 (2006).

APPENDIX: DERIVATION OF AREA-LOAD-DEPTH RELATIONS FOR ANALYSIS OF CREEP AND RELAXATION

The key to analyzing an indentation creep experiment is to be able to identify how the area increases with depth. One way to accomplish this is to measure the instantaneous contact stiffness continuously during creep then relate this stiffness back to area.[19,20] Another way is to estimate the area based on depth, which is what we have used previously.[11] Below, we present an updated method for using this latter approach. Previously, it was argued that the area-plastic depth relation during creep can be obtained using the usual area function. This is equivalent to assuming $\zeta_p \equiv d \ln \sqrt{A} \,/\, d \ln h_\mathrm{p} = 1$ for a pyramid-shaped indenter. However, our finite element analysis and experimental results show that in general $\zeta_p \neq 1$.

Although this work is predominantly concerned with constant load creep, we shall formally allow P to vary in the analysis so that the analysis is capable of handling the non-ideal situation where P changes a little during a test due to instrumental effects. For instance, the BNC test works best when the Triboindenter is run in open loop control, in which case the load changes by a small amount during the experiment. Furthermore, the analysis is capable of handling the more general case where P is intentionally allowed to change, such as in the load relaxation test, where the depth is held fixed while the load is allowed to relax.[11]

At any instant during the experiment, the plastic component of the indenter depth will be the total depth less the elastic contribution

$$h_{\mathrm{p}} = h_{\mathrm{t}} - \frac{P}{E_{\mathrm{eff}}\sqrt{A}} \quad . \tag{A1}$$

The second term on the right side of Eq. (A1) is the compliance of specimen-indenter contact for the material immediately adjacent to the indent, with $E_{\mathrm{eff}} = \beta E^*$. It has been assumed in this formula that the machine and structural compliances[32] have been removed from the measurement. In its current form, Eq. (A1) cannot be used to calculate h_{p} from measured load, P, and total depth, h_{t}, because A at each point during the experiment is unknown. To solve this problem, we use an approximation. To first order, $1/\sqrt{A} \cong (1/\sqrt{A^0})\left(1 - \Delta \ln \sqrt{A}\right)$ where A^0 is the area at unloading and $\Delta \ln \sqrt{A} = (A - A^0)/2A^0$. We have

$$h_{\mathrm{p}} \cong h_{\mathrm{t}} - \frac{P}{E_{\mathrm{eff}}\sqrt{A^0}}\left(1 - \Delta \ln \sqrt{A}\right) \quad . \tag{A2}$$

Changes in $\sqrt{A}$ in (A2) derive from changes in C^p and h_{p} as evident from Eq. (8). Substituting $\Delta \ln H = \Delta \ln P - \Delta \ln A$ into Eq. (9), then employing some algebraic manipulation along with Eq. (10) gives

$$\Delta \ln \sqrt{A} = \frac{1}{2}(1 - \zeta_i)\Delta \ln P + \zeta_i \Delta \ln h_i \quad . \tag{A3}$$

We may then substitute this expression with $i \to p$ into Eq. (A2) to obtain

$$h_{\mathrm{p}} \cong h_{\mathrm{t}} - \frac{P}{E_{\mathrm{eff}}\sqrt{A_0}}\left(1 - \frac{1}{2}\left(1 - \zeta_p\right)\Delta \ln P - \zeta_p \Delta \ln h_{\mathrm{p}}\right) \quad . \tag{A4}$$

Finally, $\Delta \ln h_{\mathrm{p}} \approx (h_{\mathrm{p}} - h_{\mathrm{p}}^0)/h_{\mathrm{p}}^0$, where h_{p}^0 is the plastic depth immediately prior to unloading. Rearrange terms and solving for h_{p} gives

$$h_{\mathrm{p}} \cong h_{\mathrm{p}}^0 + \frac{h_{\mathrm{t}} - h_{\mathrm{p}}^0 - \dfrac{P}{E_{\mathrm{eff}}\sqrt{A^0}}\left(1 - \left(1 - \zeta_p\right)\dfrac{P - P^0}{2P^0}\right)}{1 - \dfrac{P\zeta_p}{h_{\mathrm{p}}^0 E_{\mathrm{eff}}\sqrt{A^0}}} \quad , \tag{A5}$$

where P^0 is the load immediately prior to unloading. In the analysis of creep data Eq. (A5) is used to determine h_{p} as a function of time from instantaneous load (P) and depth (h_{t}) data; Eq. (A3) is then used to determine the changes in the area of the indent as a function time. With the exception of ζ_p, all of the parameters on the right side of Eq. (A5) can be measured from a load-depth trace.

A critical assumption in the analysis is that the indenter is a perfect cone or pyramid. Experiments should be analyzed consistent with that assumption. In practice, it is necessary for a Berkovich tip that the indents for creep analysis be placed deeper than the bluntness of the tip. Even for deep indents, it is also necessary to account for the bluntness of the tip by adjusting the depths accordingly. For instance, for one of the Berkovich indenters used in this work the $\sqrt{A}$-h_{t} profile for deep indents can be approximated with a straight line that intercepts the depth axis at -16 nm. In this case the tip bluntness is 16 nm, which is added to the measured values of depth (h_{t}) prior to performing the analysis. All other calculations follow from there.

In practice, an experimenter might wish to work with h_{c} or h_{t} rather than h_{p} as we have done. The h_{c} is defined as

$$h_{\mathrm{c}} = h_{\mathrm{t}} - \in P\left(\frac{1}{E_{\mathrm{eff}}\sqrt{A}}\right) \quad , \tag{A6}$$

where $\in$ is the indenter shape factor of Oliver and Pharr,[17] usually taken to be about 0.72. Using arguments similar to the ones used to derive Eq. (A5), we may estimate h_{c} as a function of time during creep or load relaxation based on

$$h_{\mathrm{c}} \cong h_{\mathrm{c}}^0 + \frac{h_{\mathrm{t}} - h_{\mathrm{c}}^0 - \dfrac{\in P}{E_{\mathrm{eff}}A^0}\left(1 - (1 - \zeta_c)\dfrac{P - P^0}{2P^0}\right)}{1 - \dfrac{\in P\zeta_c}{E_{\mathrm{eff}}A^0 h_{\mathrm{c}}^0}} \quad . \tag{A7}$$

Once the contact depth is determined as a function of time, the change in area may be estimated using Eq. (A3) with $i = c$. To analyze creep based on total depth, Eq. (A3) with i = t to calculate the area. Although in principle this is the easiest approach, it is also likely to be the one that is most subject to error because ζ_t has a wider variation than either ζ_c or ζ_p.